Specialty Journal of Pharmacognosy, Phytochemistry, and Biotechnology
ISSN: 3062-441X
2023, Volume 3, Page No: 142-163

Available online at: www.galaxypub.co/page/journals

Galaxy Publication

Regulation of Lung Adenocarcinoma Metastasis by AH-6809 via NLRP7 and Prognostic Evaluation of Critical Metastasis-Associated Genes

Khalid Rahman[1], Ayesha Malik[1]*, Farhan Iqbal[1], Usman Tariq[1]

[1]Department of Pharmacognosy, Faculty of Pharmacy, University of Karachi, Karachi, Pakistan.

***E-mail** ✉ ayesha.malik.pg@gmail.com

Received: 04 August 2023; **Revised:** 27 October 2023; **Accepted:** 27 October 2023

ABSTRACT

Lung adenocarcinoma (LUAD) ranks among the deadliest cancers worldwide, with metastasis representing the primary cause of mortality. Despite advancements in diagnosis and treatment, the processes enabling LUAD cells to infiltrate the blood-brain barrier remain largely unknown. Although genomic profiling has provided insight into primary tumors, the genetic determinants and clinical significance of metastasis in LUAD are still poorly characterized. This study aims to delineate genomic differences between LUAD tumors that metastasize to the brain and those that do not, identify potential prognostic biomarkers, and investigate the modulatory effects of AH-6809 on molecular pathways governing metastasis, particularly focusing on post-translational modifications (PTMs). Data from The Cancer Genome Atlas (TCGA) and the Gene Expression Omnibus (GEO) were analyzed to detect differentially expressed genes (DEGs) between brain-metastatic and non-metastatic LUAD samples. Weighted Gene Co-expression Network Analysis (WGCNA) was applied to identify critical gene modules, and their prognostic value was assessed via Kaplan-Meier survival analysis. In vitro experiments, including CCK8 proliferation assays and qRT-PCR, were conducted to evaluate the anti-tumor effects of AH-6809, while immunofluorescence assays measured apoptosis and inflammation-related markers. Analysis revealed distinct genomic profiles between brain-metastatic and non-metastatic LUAD, identifying NLRP7, FIBCD1, and ELF5 as significant prognostic indicators. Treatment with AH-6809 suppressed LUAD cell proliferation, induced apoptosis, and altered epithelial-mesenchymal transition (EMT) marker expression. Knockdown of NLRP7 diminished these effects, highlighting its critical role in metastasis regulation. Supporting evidence from the literature demonstrated that AH-6809 exerts tumor-suppressive effects, particularly in NLRP7-deficient cells, by inhibiting growth and promoting apoptosis. AH-6809 also modulated SUMO1-dependent PTMs and reduced expression of EMT markers such as VIM and CDH2, with partial reversal observed upon NLRP7 silencing. Immunofluorescence further confirmed enhanced apoptosis and inflammatory responses in LUAD cells treated with AH-6809, especially under NLRP7 knockdown conditions. These regulatory effects appear to involve SUMO1-mediated PTMs and NQO1, warranting further investigation to fully understand the mechanisms and therapeutic potential. The findings underscore the importance of NLRP7 and associated genes in LUAD metastasis and suggest that AH-6809 represents a promising candidate for targeted therapy against brain-metastatic LUAD.

Keywords: Lung adenocarcinoma, Brain metastasis, Brain, Pan-cancer analysis, Genomic profiling, Genomic

How to Cite This Article: Rahman K, Malik A, Iqbal F, Tariq U. Regulation of Lung Adenocarcinoma Metastasis by AH-6809 via NLRP7 and Prognostic Evaluation of Critical Metastasis-Associated Genes. J Pharmacogn Phytochem Biotechnol. 2023;3:142-63. https://doi.org/10.51847/6epWrws46C

Introduction

Lung adenocarcinoma (LUAD), the most prevalent subtype of non-small cell lung cancer (NSCLC), remains a major contributor to cancer-related mortality worldwide [1, 2]. Despite considerable progress in diagnostic techniques and treatment strategies, predicting LUAD progression, particularly metastasis, continues to be challenging due to limited understanding of the molecular processes that drive metastatic spread [3, 4]. Brain metastases develop in roughly 20%–40% of patients with advanced LUAD, establishing this cancer as a leading cause of secondary brain tumors among different cancer types [5, 6]. Metastasis is a complex, multi-step process

wherein malignant cells disseminate from the primary tumor to distant sites, representing the most lethal stage of tumor progression [7, 8]. LUAD cells gain invasive and metastatic potential via epithelial-mesenchymal transition (EMT), promote angiogenesis, remodel the brain microenvironment, and evade immune responses, collectively facilitating metastatic colonization [9, 10]

Although large-scale genomic efforts, including The Cancer Genome Atlas (TCGA), have provided extensive insight into the molecular characteristics of primary LUAD tumors, the specific genetic and epigenetic mechanisms underlying brain metastasis remain poorly defined. Key alterations, such as EGFR mutations and ALK rearrangements, have been associated with increased risk of brain metastasis [4, 11]. Pan-cancer analyses offer opportunities to uncover common molecular drivers across multiple cancer types, thereby providing a broader understanding of tumor biology [7, 12]. Nevertheless, the heterogeneity and dynamic nature of metastatic LUAD complicate the identification of reliable biomarkers and therapeutic targets [13, 14]. Previous genomic studies have largely focused on primary tumors, with limited efforts to link specific genetic changes to metastatic potential [15].

While many genes have been implicated in primary LUAD tumors, their direct contributions to metastasis remain unclear [16, 17]. Genes such as ARRDC5 and ELF5 have been studied for their roles in cancer progression, yet their pan-cancer significance has not been fully explored [18, 19]. Additionally, L1CAM exhibits context-dependent behavior: although it promotes invasion in several cancers, its downregulation in LUAD metastasis demonstrates the complexity of its function across tumor types [20, 21]. Current findings highlight the need for in-depth investigation into the prognostic potential of these genes and their roles in the metastatic cascade. While some therapeutic approaches targeting these pathways exist [22, 23], their effectiveness in brain-metastatic LUAD has yet to be fully determined. Accurate molecular markers capable of predicting metastasis and guiding therapy are critical to improving patient outcomes. Although the genomic landscape of LUAD is increasingly well characterized, metastatic disease has been understudied and often analyzed using small sample sizes [10, 24]. Analyses based on large public datasets offer comprehensive coverage but may lack detailed clinical information, highlighting the need for experimental validation to confirm the functional relevance of candidate genes [25-28]. The integration of bioinformatics and big data approaches has become essential for identifying clinically relevant biomarkers for diagnosis and prognosis in LUAD [29, 30]. Investigating protein-protein interaction networks, their regulatory mechanisms, and post-translational modifications provides key insights into cellular signaling and disease regulation [31, 32]. Transcriptomic analyses have further elucidated the role of the immune microenvironment in disease progression [33-36]. By employing advanced techniques such as machine learning, multi-omics integration, and high-throughput sequencing, researchers are developing precision medicine strategies and personalized therapeutic approaches [36-38].

This study aims to address these gaps through a comprehensive genomic and bioinformatic investigation of LUAD metastasis, with a focus on brain metastases. While prior research has identified numerous genetic alterations in LUAD, few studies have specifically linked these changes to metastatic behavior, and their clinical significance remains largely unexplored. By integrating computational analyses with experimental validation, this work seeks to uncover prognostic biomarkers and therapeutic targets to improve understanding and management of brain-metastatic LUAD.

Materials and Methods

GEO dataset retrieval and preprocessing

Microarray datasets from LUAD brain metastasis samples were analyzed in this study. A total of 28 specimens were included, with 19 contributed by Marc Ladanyi's group and nine by William L. Gerald's team. The data were obtained from the Gene Expression Omnibus (GEO) under accession number GSE14108. To further investigate the tumor microenvironment in LUAD brain metastases, bulk RNA sequencing was performed on six patient-derived samples using the Illumina HiSeq X Ten platform; these sequencing datasets are available in GEO under accession number GSE141685. Differential gene expression analyses compared brain metastasis samples with primary LUAD tumors from TCGA, including 14 early-stage and 11 late-stage tumors. Multiple testing corrections were applied using the False Discovery Rate (FDR), and statistical significance was defined as $p < 0.05$. Data were normalized, and the limma R package was applied, employing linear modeling and empirical Bayes methods to identify significantly altered genes.

Pan-cancer core gene expression profiling

For comprehensive analysis, mRNA expression, DNA copy number variation (CNV), and 450K DNA methylation data were collected for 20 cancer types: BLCA, BRCA, CHOL, COAD, CESC, ESCA, GBM, HNSC, KICH, KIRC, KIRP, LIHC, LUAD, LUSC, PAAD, PRAD, READ, STAD, THCA, and UCEC. Tumor and normal tissue data were sourced from Firehose (http://gdac.broadinstitute.org), while mutation, miRNA, and clinical data were retrieved via the Xena Browser (https://xenabrowser.net/datapages/). Gene expression differences between tumor and normal samples were evaluated using the Wilcoxon rank-sum test, with $\alpha = 0.05$. TPM-normalized expression values for tumors (TCGA) and normal tissues (GTEx) were obtained through UCSC Xena and standardized using z-scores to reduce dataset variability. Both heterozygous and homozygous CNV alterations were included, and Pearson correlation coefficients were calculated to quantify the relationship between gene expression and CNV segments.

Promoter methylation analysis of core genes

DNA methylation levels were examined for multiple promoter regions: TSS1500 (1,500 bp upstream of the transcription start site), TSS200 (within 200 bp of the TSS), the first exon, and the 5' untranslated region (5'UTR). Median methylation values across these regions were computed to generate an overall methylation index for each sample. Associations between promoter methylation and gene expression were assessed using Spearman's rank correlation, a non-parametric method suitable for evaluating monotonic relationships in non-normal distributions. Additionally, methylation differences between tumor and normal tissues were assessed using the Wilcoxon rank-sum test to identify substantial shifts in DNA methylation patterns.

ATAC-seq analysis of core genes

ATAC-seq datasets were analyzed using the ChIPseeker package. Transcription start site (TSS) regions in gene promoters were annotated using the annotatePeak function, with the tssRegion parameter set to c(-3,000, 3,000) to cover 3 kb upstream and downstream of each TSS. This approach enabled detailed mapping of transcription factor binding sites and histone modification patterns. Genome-wide coverage plots were generated using the covplot function, displaying peak distribution across the genome and providing detailed information on gene names, chromosomal location, cancer types, and distances from TSSs. These visualizations allowed for both global assessment of open chromatin landscapes and focused examination of regulatory features around specific gene promoters.

GSEA enrichment analysis in pan-cancer studies

RNA-seq and microarray datasets for multiple cancer types were obtained from the TCGA database, including both tumor and corresponding normal (or paired) samples. All datasets underwent stringent quality control procedures to ensure sample integrity and probe accuracy. Standardization was applied to minimize technical biases across datasets. Differential gene expression was analyzed using the R packages limma and clusterProfiler, which perform background correction, normalization, and statistical testing to identify significantly altered genes. Genes were selected based on log2 fold change (log2FC), reflecting the magnitude of expression change, and p-values, indicating statistical significance. Subsequently, the clusterProfiler package was used to perform pathway enrichment analyses via Gene Set Enrichment Analysis (GSEA) against KEGG, GO, and Reactome databases. The enrichment score (ES), ranging from 0 to 1, quantified the association between biological pathways and observed gene expression changes. Visualization of results, including bar charts, scatter plots, and heatmaps, was performed using the ggplot2 R package, providing clear and interpretable representations of the data. This analytical workflow enables systematic investigation of molecular mechanisms driving cancer-associated gene expression patterns.

Molecular characterization of core genes in LUAD

The diagnostic utility of the single-sample Gene Set Enrichment Analysis score (ssGSEA score) for distinguishing LUAD from normal tissues was assessed using receiver operating characteristic (ROC) curve analysis via the pROC R package. The analysis calculated the area under the curve (AUC) with 95% confidence intervals and produced smoothed ROC plots. ssGSEA scores were derived from TCGA RNA-seq data using the GSVA package's "ssgsea" function. Expression data were obtained from PanCanAtlas (EBPlusPlusAdjustPANCAN_IlluminaHiSeq_RNASeqV2) processed through the Firehose pipeline with

MapSplice + RSEM and normalized to an upper quartile of 1,000. Comparisons of ssGSEA scores between tumor and normal tissues were conducted using the Wilcoxon rank-sum test, while paired tumor versus adjacent non-tumor tissue differences were assessed using the Wilcoxon signed-rank test. Calibration curves evaluated the agreement between predicted and observed values, and goodness-of-fit tests examined model performance. Differences in ssGSEA scores across early- and late-stage LUAD samples were assessed using the Wilcoxon rank-sum test, followed by Kruskal-Wallis rank-sum testing to determine the likelihood that observed differences arose by chance. These analyses provide robust statistical insights into the relationship between gene set expression and clinical features in LUAD.

Survival prognosis analysis of core genes in LUAD

Kaplan-Meier survival analysis was performed in R using the survival package to stratify patients into high- and low-ssGSEA score groups, with cut-off values optimized to ensure each group represented at least 30% of the cohort. Survival differences between groups were evaluated using the log-rank test through the survfit function, while univariate Cox regression analyses were combined via inverse variance meta-analysis to calculate hazard ratios as primary outcome measures.

Connectivity map (cMAP) analysis

To explore potential therapeutic compounds capable of counteracting tumor-promoting effects of specific genes, Connectivity Map (cMAP) analysis was performed using CMAP gene signatures. The dataset included gene expression profiles for 1,288 compounds. Gene signatures were constructed by selecting the 150 most significantly upregulated and 150 most significantly downregulated genes based on high versus low gene expression comparisons in tumors. The eXtreme Sum (XSum) algorithm was used to compare these signatures with cMAP reference profiles, generating similarity scores for all compounds. This analysis followed established methodologies described in previous studies [39, 40].

Cell Lines and clinical specimens

The non-small cell lung cancer (NSCLC) cell line NCI-H1299 (ATCC® CRL-5803™) was acquired from the American Type Culture Collection (ATCC, USA). Cells were maintained in Dulbecco's Modified Eagle Medium (DMEM) supplemented with 10% fetal bovine serum (FBS) under standard culture conditions.

Lentiviral-mediated NLRP7 knockdown

To investigate the functional role of NLRP7, gene silencing was performed using lentiviral vectors targeting NLRP7. Specific sequences for gene knockdown were obtained from Open Biosystems, and transduced cells were used for downstream functional assays.

Immunofluorescence staining

Cells were seeded in 24-well plates and allowed to adhere overnight. Fixation was carried out with 3.7% paraformaldehyde at room temperature for 15 minutes, followed by permeabilization in chilled methanol at −20°C for 15 minutes. Blocking was performed for 1 hour in PBS containing 5% normal goat serum and 0.5% Triton X-100. Primary antibodies were applied and incubated overnight at 4°C. After three washes with PBS (10 minutes each), cells were treated with fluorophore-conjugated goat anti-rabbit secondary antibodies (1:500 dilution) at room temperature. Nuclei were counterstained with DAPI (Sigma, D9542) for 30 minutes prior to imaging. Fluorescence images were captured using a Nikon Eclipse E800 microscope.

Quantitative real-time PCR (qRT-PCR)

Total RNA was extracted using TRIzol reagent, and cDNA was synthesized with the PrimeScript™ RT Reagent Kit (TaKaRa, Japan) in combination with the FastStart Universal SYBR Green Master (ROX; Roche, Switzerland). qRT-PCR was performed on a Bio-Rad CFX96™ Real-Time System with a C1000™ Thermal Cycler to quantify gene expression.

Cell proliferation assay (CCK-8)

Cell proliferation was measured using the CCK-8 assay. Briefly, 2,000 cells were seeded per well in a 96-well plate and incubated at 37°C with 5% CO_2. Ten microliters of CCK-8 solution (Vazyme Biotech Co., Ltd.) were

added per well, followed by 2 hours of incubation at 37°C. Absorbance at 450 nm was measured using a microplate reader, and proliferation curves were constructed from three independent experiments.

Colony formation assay

Long-term proliferative capacity was assessed via a plate colony formation assay. LUAD cells were either transfected with shRNA targeting NLRP7 or treated with AH-6809. Cells (500 per well) were seeded into six-well plates and cultured at 37°C under 5% CO_2, with medium refreshed every three days. After 10–14 days, visible colonies were fixed with 4% paraformaldehyde for 15 minutes and stained with 0.1% crystal violet for 30 minutes. Colonies containing more than 50 cells were counted under a microscope, and colony formation efficiency was calculated as the percentage of plated cells forming colonies. Experiments were conducted in triplicate, and statistical significance was determined using Student's t-test.

Statistical analyses

Data are presented as mean ± standard deviation (SD). Statistical analyses were conducted using GraphPad Prism version 8. Comparisons between two groups were performed with a t-test, while one-way ANOVA was used for multi-group comparisons. Correlations were assessed with Pearson's correlation coefficient, and p-values <0.05 were considered statistically significant.

Results and Discussion

Differential expression analysis of LUAD brain metastasis

To identify genes associated with brain metastasis in LUAD, GEO datasets were analyzed. Significant differences in gene expression were observed between primary LUAD tumors and brain metastasis samples. Principal component analysis (PCA) further highlighted the separation between primary and metastatic samples. The volcano plot **(Figure 1a)** revealed key upregulated genes in brain metastases, including SLC7A10, SFT2D3, KTI12, and MIR1244-1, as well as downregulated genes. Heatmap visualization of normalized expression values **(Figure 1b)** demonstrated clear clustering of primary versus metastatic samples, with metastatic samples showing distinct regulatory patterns (highlighted in cyan). These results pinpoint potential molecular targets for therapeutic intervention and underscore the importance of understanding the mechanisms underlying LUAD brain metastasis.

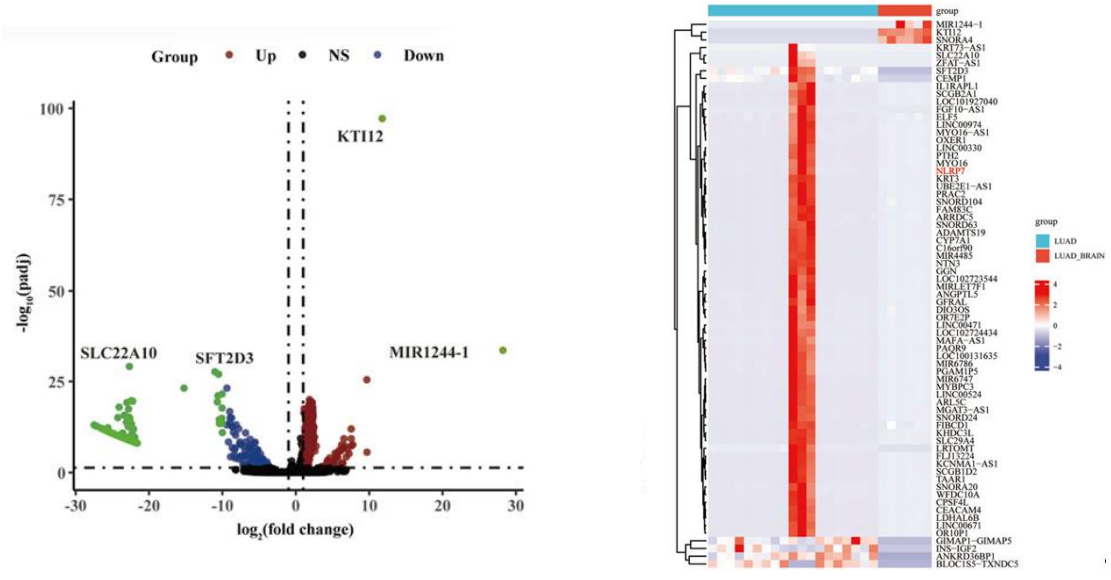

a) b)

Figure 1. Identification of Genes Linked to LUAD Brain Metastasis from GEO Data. (a) Volcano plot showing differential gene expression between primary lung adenocarcinoma (LUAD) and LUAD brain metastasis (LUAD_brain) samples. The x-axis represents the log2-transformed fold changes, and the y-axis shows -log10 of the p-values. Genes significantly elevated in brain metastases are colored red, downregulated genes in green, non-significant genes in black, and unchanged genes in blue. Highlighted genes include

SLC7A10, SFT2D3, KTI12, and MIR1244-1. (b) Heatmap illustrating the expression patterns of the top differentially expressed genes across LUAD and LUAD_brain samples. Normalized expression levels are indicated by a color gradient from blue (low) to red (high). Genes were clustered hierarchically based on their expression profiles, and sample groups are annotated at the top with LUAD in red and LUAD_brain in cyan.

Functional enrichment analysis of LUAD brain metastasis-related genes

To investigate the biological significance of genes linked to LUAD brain metastasis, we performed enrichment analyses. GO term analysis identified the top 10 terms within Biological Process (BP), Cellular Component (CC), and Molecular Function (MF) categories. Enriched BP terms included processes such as bile acid biosynthesis, metabolism of organic hydroxy compounds, and sperm plasma membrane organization. CC terms involved mitochondria and synaptic membranes, while MF terms highlighted activities like bile acid transmembrane transport, organic hydroxy compound transport, and mRNA 3′-end processing **(Figure 2a).** KEGG pathway analysis further revealed significant enrichment in neuroactive ligand-receptor interactions, microRNAs in cancer, fat digestion and absorption, and olfactory transduction pathways **(Figure 2b)**. Chord diagrams **(Figures 2c and 2d)** mapped the relationships between enriched GO terms or KEGG pathways and their associated genes, highlighting overlapping and unique gene sets across functional categories. Collectively, these analyses provide a comprehensive view of the molecular mechanisms and pathways potentially driving LUAD brain metastasis, offering a foundation for identifying therapeutic targets and understanding disease progression.

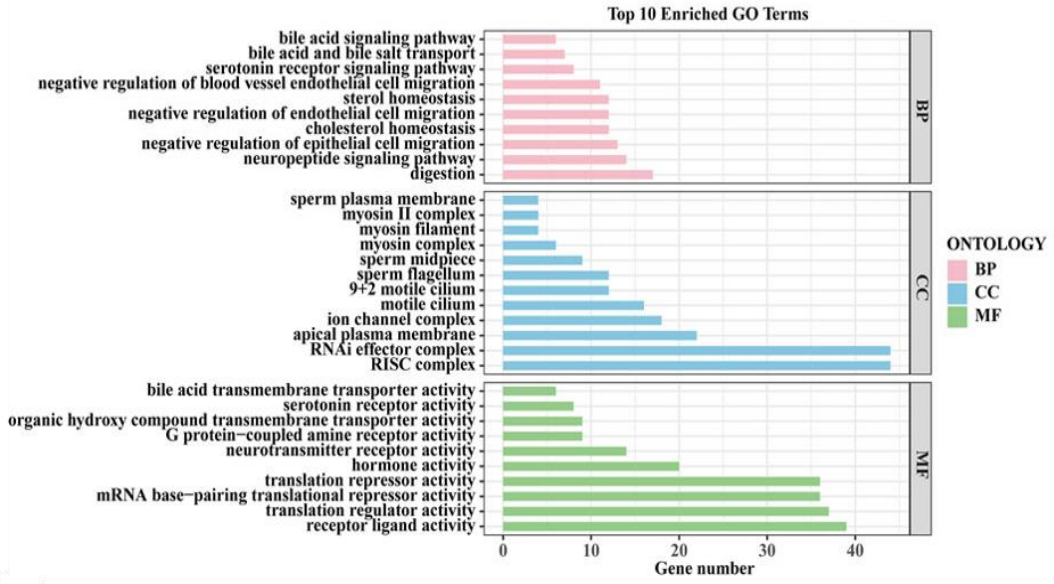

a)

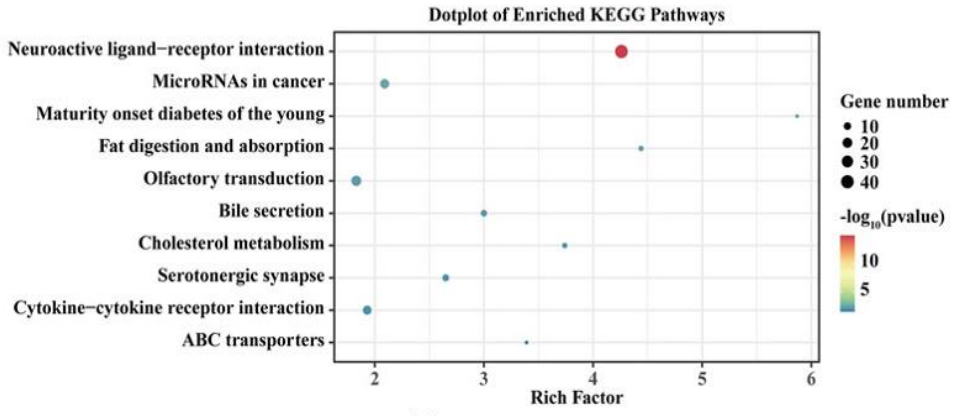

b)

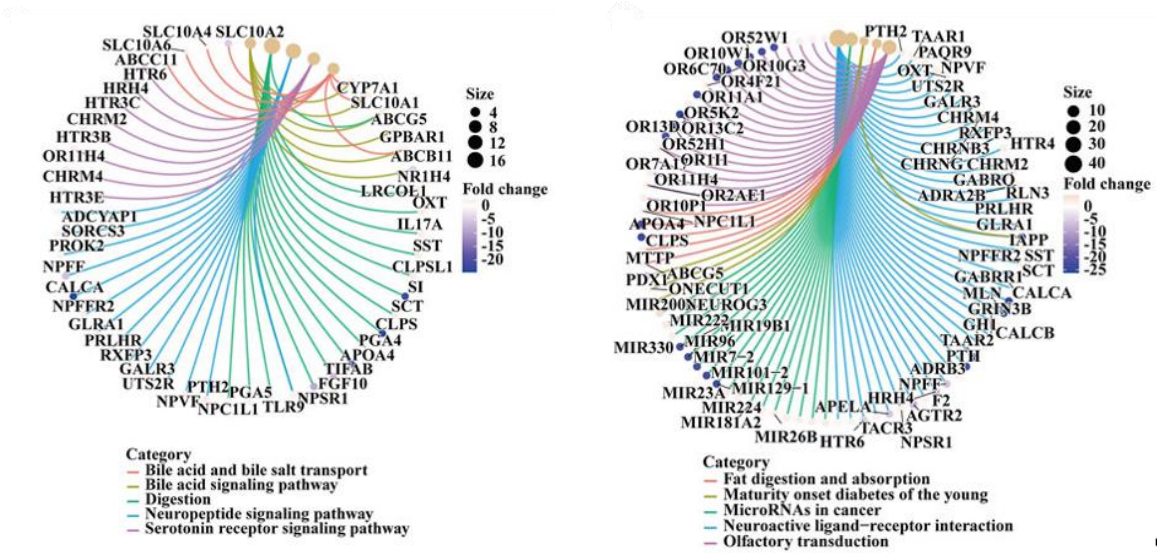

c) d)

Figure 2. Functional Enrichment and Pathway Analysis of LUAD Brain Metastasis Genes from GEO Data. (a) The bar chart highlights the ten most significantly enriched Gene Ontology (GO) terms identified in genes implicated in lung adenocarcinoma (LUAD) brain metastasis, classified into Biological Process (BP), Cellular Component (CC), and Molecular Function (MF) categories. The y-axis lists GO terms, while the x-axis indicates the number of genes contributing to each term. BP terms included processes such as bile acid biosynthesis, hydroxy compound metabolism, and sperm plasma membrane organization. CC terms were predominantly linked to mitochondria and synaptic membranes, whereas MF terms involved bile acid transport activity, transmembrane hydroxy compound transport, and mRNA 3′-end processing. Significance was calculated using adjusted p-values from GEO-derived data. (b) KEGG pathway enrichment for LUAD brain metastasis-related genes is illustrated in a dot plot. Pathways are listed on the y-axis, with the x-axis representing the enrichment ratio (rich factor). Dot size corresponds to the number of mapped genes, and dot color indicates statistical significance. Prominent pathways include neuroactive ligand-receptor interaction, microRNAs in cancer, fat digestion and absorption, and olfactory transduction. (c) A chord diagram depicts connections between enriched GO terms and their associated genes, revealing both shared and unique gene-function relationships to provide insight into biological roles in brain metastasis. (d) Another chord diagram demonstrates relationships between KEGG pathways and their associated genes, highlighting complex interconnections and unique gene contributions across pathways.

Identification of L1CAM-associated prognostic genes in LUAD brain metastasis

Weighted Gene Co-Expression Network Analysis (WGCNA) was conducted to uncover L1CAM-related prognostic genes. Hierarchical clustering of LUAD and brain metastasis samples was used to identify outliers and examine sample groupings. Network topology assessments confirmed scale-free properties, as shown by scale independence and mean connectivity plots. Analysis of node connectivity highlighted key hub genes exerting central regulatory influence. Module eigengene clustering identified highly correlated gene modules, elucidating co-expression patterns across primary and metastatic LUAD samples. Correlation analysis between modules and clinical traits showed weak negative associations in the turquoise module and stronger negative associations in the grey module **(Figure 3a)**. The dendrogram of genes with module color assignments is presented in **Figure 3b**. Scatterplots and correlation matrices confirmed robust associations between module eigengenes, with correlation coefficients reaching 0.99 **(Figure 3c)**. Integration of WGCNA modules with differentially expressed genes revealed 534 overlapping genes **(Figure 3d)**. From these, six key prognostic genes associated with L1CAM were identified (L1CAM, ARRDC5, NLRP7, ELF5, LINC00494, FIBCD1) **(Figure 3e)**. Network analysis illustrated strong interactions among these genes **(Figure 3f)**, suggesting a collaborative role in promoting LUAD brain metastasis.

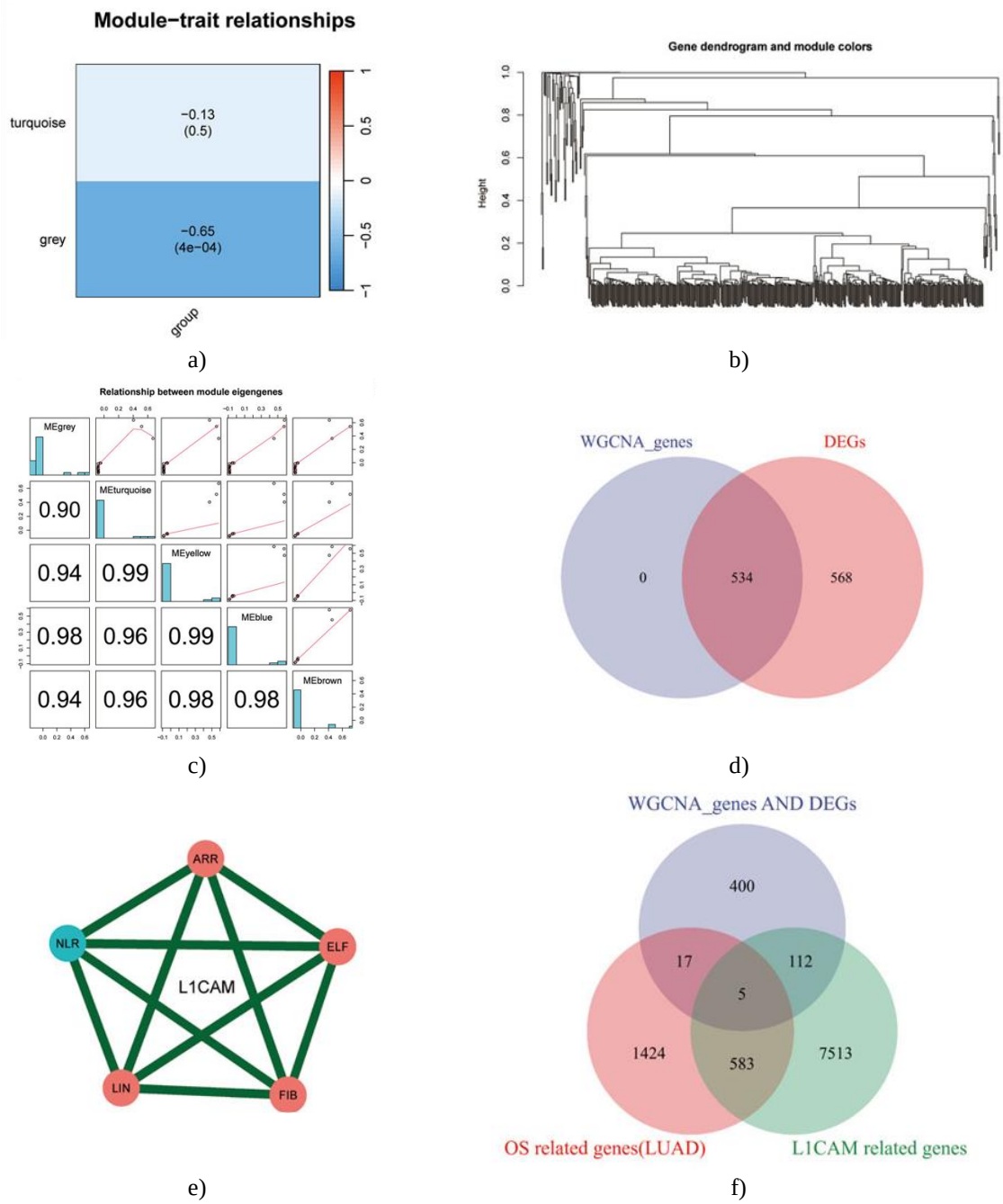

Figure 3. WGCNA identifies five L1CAM-associated prognostic genes in lung cancer brain metastasis. (a) The heatmap displays correlations between WGCNA-identified modules and the clinical trait (group). The turquoise module exhibits a weak negative correlation (−0.13, p = 0.5), while the grey module shows a stronger negative correlation (−0.65, p < 0.001), indicating a meaningful association. (b) Hierarchical clustering dendrogram of genes, with each color representing a distinct co-expression module as determined by WGCNA, reflecting highly interconnected gene clusters. (c) Correlation matrices and scatter plots of module eigengenes highlight strong co-expression patterns, with correlation values reaching up to 0.99. (d) A comparison between WGCNA-identified genes (left circle) and DEGs (right circle) reveals 534 overlapping genes, suggesting their potential relevance to the trait under study. (e) Venn diagram showing overlaps among WGCNA genes (blue), DEGs (pink), and L1CAM-related genes (green). The central intersection identifies five common genes, likely key prognostic markers for brain metastasis in lung cancer. (f) Interaction network of the five selected L1CAM-related prognostic genes (L1CAM, ARRDC5, NLRP7, ELF5, LINC00494, FIBCD1) illustrates strong connections (green edges), indicating cooperative roles in metastasis.

Pan-cancer expression profiling of core genes

We analyzed the expression landscape of seven core genes (ARRDC5, ELF5, FIBCD1, LINC00494, NLRP7, L1CAM) across multiple cancer types, using both unpaired and paired sample datasets from TCGA-GTEx. The heatmap of unpaired samples **(Figure 4a)** revealed pronounced differences in expression across cancers. For example, L1CAM was significantly overexpressed in lung squamous cell carcinoma (LUSC), while ARRDC5 showed elevated levels in breast invasive carcinoma (BRCA), suggesting their involvement in tumorigenesis. Paired sample analysis **(Figure 4b)** compared tumor and adjacent normal tissues to reduce inter-patient variability; notable downregulation of ELF5 in colon adenocarcinoma (COAD) implies a potential tumor-suppressive role, whereas NLRP7 and ARRDC5 remained consistently dysregulated, reinforcing their therapeutic relevance.

Using TCGA-GTEx datasets for broader analysis, bar and dot plots **(Figure 4c)** summarized the number of cancers with significant up- or downregulation for each gene. ARRDC5 and NLRP7 were the most consistently dysregulated across multiple cancers, highlighting their central role in tumor biology. Copy number variation (CNV) analysis **(Figure 4d)** showed that ARRDC5 and L1CAM undergo frequent CNV alterations, likely contributing to their differential expression and oncogenic potential. Correlation analysis between CNV and expression **(Figure 4e)** indicated a positive relationship, exemplified by ARRDC5 in BRCA, supporting the role of genomic alterations in regulating gene activity.

Functional enrichment analysis using GSEA revealed that these dysregulated genes are associated with key biological pathways, including apoptosis, immune response, and cell cycle regulation **(Figure 4f)**. In particular, NLRP7 was linked to immune-related pathways, suggesting its influence on the tumor immune microenvironment. Tumor microbiome analysis across cancers **(Figure 4g)** highlighted potential interactions between microbial species and gene expression, with certain microbes more abundant in lung and gastrointestinal tumors, potentially modulating observed gene expression patterns.

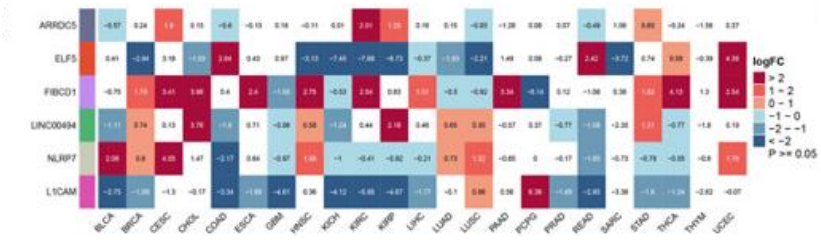

a)

b)

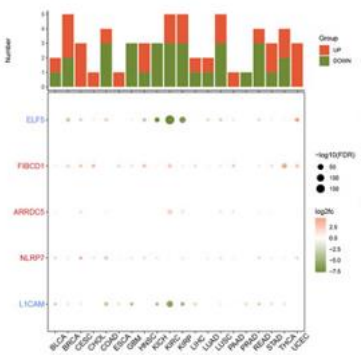

c)

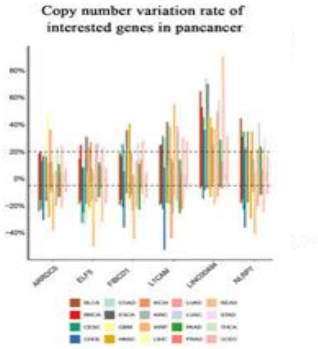

d)

e) f)

g)

Figure 4. Pan-cancer profiling of core gene expression, copy number alterations, and functional enrichment. (a) Heatmap depicting the differential expression of six core genes (ARRDC5, ELF5, FIBCD1, LINC00494, NLRP7, L1CAM) across multiple cancer types using unpaired samples. The log fold change (logFC) indicates expression differences between tumor and normal tissues, with red representing upregulation and blue showing downregulation. Significant differences are denoted by $p < 0.05$. (b) Heatmap showing differential expression of the same genes in paired tumor and adjacent normal tissues, aiming to minimize inter-patient variability, using the same color scheme as panel A. (c) Combined bar and dot plots summarizing TCGA-GTEx dataset analysis. The bar plot shows the number of cancer types with significant upregulation (red) or downregulation (blue) for each gene, while the dot plot illustrates logFC values across cancers; dot size reflects statistical significance (-log10(FDR)). (d) Boxplot representing copy number variation (CNV) rates of core genes across cancer types, highlighting genes with notable CNV alterations. (e) Bubble plot depicting correlations between CNV and gene expression; larger bubbles represent stronger correlations. (f) GSEA results for core genes, where dot size represents enrichment significance (-log10(p-value)) and color indicates enrichment direction (red = positive, blue = negative). (g) Heatmap showing tumor-associated microbial species abundance across cancers, providing insights into potential interactions between the tumor microbiome and gene expression patterns.

Promoter methylation and correlation with gene expression

This analysis revealed clear distinctions between LUAD primary tumors and brain metastasis samples, with significant clustering differences. The heatmap of promoter methylation levels demonstrated wide variability, with blue cells indicating low methylation and red cells representing high methylation. Notably, ARRDC5 and NLRP7 showed prominent differences between primary and metastatic tissues. Correlation analysis explored the association between mRNA expression and promoter methylation for the core genes, confirming that methylation levels influence gene expression.

Detailed promoter methylation profiling of core genes

Promoter regions of six core genes were analyzed to determine methylation patterns. For each gene, methylation peaks were mapped, and their distribution across genomic features was assessed. ARRDC5 exhibited hypermethylation in 60% of the promoter and hypomethylation in 20%, with peaks concentrated mainly in exons and promoter regions. ELF5 showed balanced methylation with distinct peaks in CpG islands and promoters. FIBCD1 displayed predominantly high methylation, with 70% hypermethylated and prominent promoter peaks. L1CAM had moderate methylation, with 60% hypermethylation and peaks in CpG-rich promoter regions. LINC00494 showed high hypermethylation (80%) concentrated in both promoter and gene body regions. NLRP7 exhibited extensive hypermethylation (90%), with pronounced peaks within the promoter. These results highlight distinct promoter methylation landscapes across core genes, with hypermethylation being a common feature, suggesting a significant role in transcriptional regulation.

Correlation of core gene expression with LUAD prognosis

The association between ssGSEAscore levels and LUAD prognosis was examined. Calibration curves and goodness-of-fit assessments confirmed a reliable model for predicting tumor versus normal tissue groups, with the Hosmer-Lemeshow test showing $p = 0.555$. Differential expression analysis indicated that ssGSEAscore was significantly elevated in LUAD tumors compared to normal tissues, although paired analyses between tumor and adjacent normal samples showed no significant difference ($p = 0.559$). Expression patterns of ssGSEAscore across clinical stages I–IV were visualized with violin plots, demonstrating variability with disease progression. When early-stage (I–II) and late-stage (III–IV) groups were compared, ssGSEAscore differed significantly, suggesting its potential link to disease advancement. Median ssGSEAscore values plotted across stages revealed trends of expression with increasing disease severity. ROC curve analysis for distinguishing tumors from normal tissues yielded an AUC of 0.574 (95% CI: 0.506–0.640), reflecting moderate diagnostic performance. Collectively, these findings indicate ssGSEAscore as a potential biomarker for LUAD prognosis and highlight its variation across disease stages.

Survival prognosis analysis of core genes in LUAD

The prognostic value of core gene expression in LUAD was assessed via Kaplan-Meier survival analyses and meta-analysis. Stratification by high versus low expression levels showed no statistically significant differences in Overall Survival (OS, $p = 0.327$) **(Figure 5a)**, Disease-Specific Survival (DSS, $p = 0.195$) **(Figure 5b)**, Disease-Free Interval (DFI, $p = 0.453$), **(Figure 5c)**, or Progression-Free Interval (PFI, $p = 0.261$), **(Figure 5d)**. Validation in the GSE68465 cohort indicated a significant OS difference ($p = 0.044$), **(Figure 5e)**, whereas the GSE72094 cohort did not show significance ($p = 0.383$), **(Figure 5f)**. A meta-analysis of univariate Cox regression across multiple datasets, including GSE68465-OS, GSE72094-OS, TCGA-LUAD-OS, TCGA-LUAD-DSS, TCGA-LUAD-DFI, and TCGA-LUAD-PFI, yielded a combined hazard ratio (HR) of 1.17 (95% CI: 0.85–1.48) with no evidence of significant heterogeneity **(Figure 5i)**. These results suggest that the prognostic relevance of core gene expression in LUAD may vary depending on the dataset, underscoring the importance of context-specific interpretation. Overall, the integration of Kaplan-Meier curves and meta-analytic data provides a comprehensive assessment of the core genes' potential impact on LUAD patient outcomes.

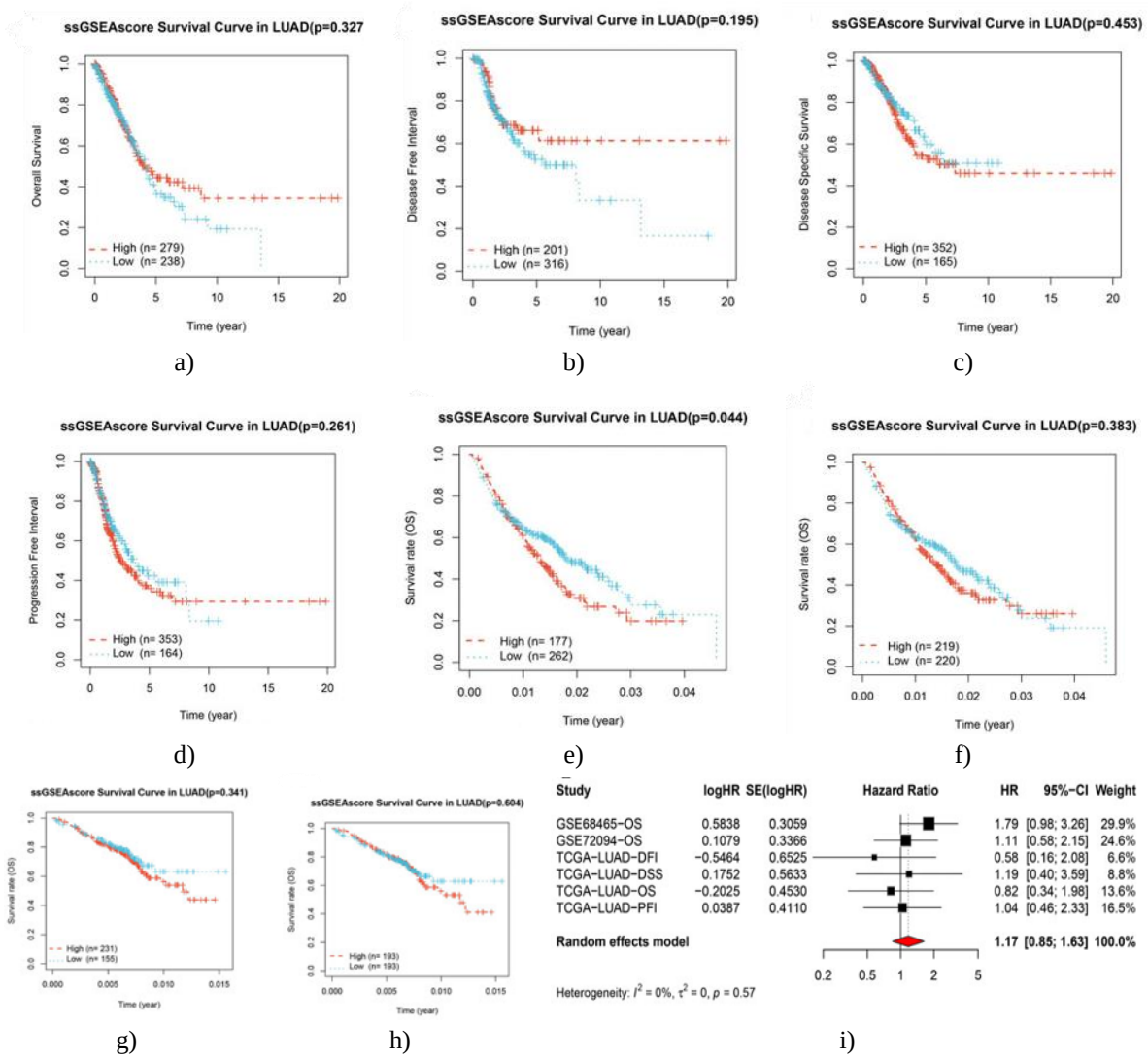

Figure 5. Prognostic evaluation of core genes in LUAD. Kaplan-Meier survival analyses were conducted to assess the impact of core gene expression on multiple survival outcomes in LUAD, including Overall Survival (OS), Disease-Specific Survival (DSS), Progression-Free Interval (PFI), and Disease-Free Interval (DFI). Patients were stratified into high and low expression groups (red: high, blue: low), with sample sizes noted for each comparison. OS (a) showed no significant difference (p = 0.327, high n = 279, low n = 314), and similar non-significant trends were observed for DSS (b, p = 0.195, high n = 201, low n = 234), DFI (c, p = 0.453, high n = 363, low n = 378), and PFI (d, p = 0.261, high n = 353, low n = 388). Additional analyses using the GSE68465 (e, p = 0.044, high n = 177, low n = 222) and GSE72094 (f, p = 0.383, high n = 219, low n = 228) datasets further evaluated OS based on core gene levels, supported by Kaplan-Meier curves (g, h). A meta-analysis of univariate Cox models (I) combined multiple datasets (GSE68465-OS, GSE72094-OS, TCGA-LUAD-OS, DSS, DFI, and PFI) to calculate overall hazard ratios (HR) with 95% confidence intervals, while heterogeneity was assessed using I^2 and associated p-values.

Pan-cancer GSVA enrichment of core genes

To explore core gene activity across cancers, a pan-cancer GSVA enrichment was performed comparing tumors and normal tissues using four computational approaches: combined z-scores, GSVA z-scores, PLAGE, and ssGSEA. This analysis revealed significant dysregulation in multiple tumor types, including GBM, THCA, PRAD, KIRP, BRCA, KIRC, BLCA, and COAD, indicating either increased or decreased expression relative to normal tissues. For instance, combined z-scores highlighted pronounced differences in GBM (p = 6.1e-04) and PRAD (p = 2.6e-16). GSVA, PLAGE, and ssGSEA analyses corroborated these findings, showing notable alterations in GBM, THCA, and KIRC. Overall, these results underscore the variable expression of core genes

across cancers, suggesting their involvement in tumor biology and potential utility as biomarkers for diagnosis or therapeutic targeting.

AH-6809 inhibits LUAD progression through modulation of apoptosis and EMT pathways

This study focused on brain-metastatic LUAD and the role of NLRP7 to unravel the molecular mechanisms by which AH-6809 suppresses LUAD metastasis. Initial high-throughput screening of a chemical library identified AH-6809 as a compound capable of interfering with oncogenic signaling pathways, prompting further investigation **(Figures 6a and 6b).** The effect of AH-6809 on LUAD cell proliferation was evaluated using a CCK8 assay, which revealed a significant, time-dependent decrease in cell viability, most pronounced at 72 and 96 hours post-treatment **(Figure 6c)**.

To explore the underlying molecular changes, qRT-PCR analysis was performed to examine apoptotic and epithelial-mesenchymal transition (EMT) markers. AH-6809 treatment led to robust upregulation of pro-apoptotic genes (BAX, Caspase-3) and inflammatory cytokine TNFα, along with a marked downregulation of EMT markers VIM and CDH2, compared to untreated controls ($p < 0.001$) **(Figure 6d).** The contribution of NLRP7 was further assessed through shRNA-mediated knockdown, which effectively reduced NLRP7 expression as confirmed by qRT-PCR ($p < 0.001$) **(Figure 6e)**. Interestingly, the combination of NLRP7 knockdown and AH-6809 partially reversed the drug's anti-proliferative effects, indicating a complex interplay between AH-6809 and NLRP7-regulated pathways **(Figure 6f)**.

Colony formation assays demonstrated that NLRP7 knockdown enhanced the tumorigenic potential of LUAD cells, whereas AH-6809 treatment strongly suppressed colony formation. Notably, this inhibitory effect was partially alleviated when NLRP7 was silenced **(Figure 6h)**. Immunofluorescence analysis revealed that AH-6809 altered the expression of inflammatory marker NQO1 and anti-apoptotic protein SUMO1, with co-staining alongside DAPI showing increased apoptosis and inflammation, particularly in cells treated with both AH-6809 and shNLRP7 **(Figure 6i)**.

Collectively, these results indicate that AH-6809 exerts substantial anti-tumor activity in LUAD by regulating apoptotic and EMT pathways. The drug appears to counteract the pro-tumorigenic effects associated with NLRP7 dysregulation, promoting tumor-suppressive outcomes **(Figure 7)**. These findings support the potential of targeting NLRP7 with AH-6809 as a therapeutic strategy for managing brain-metastatic LUAD.

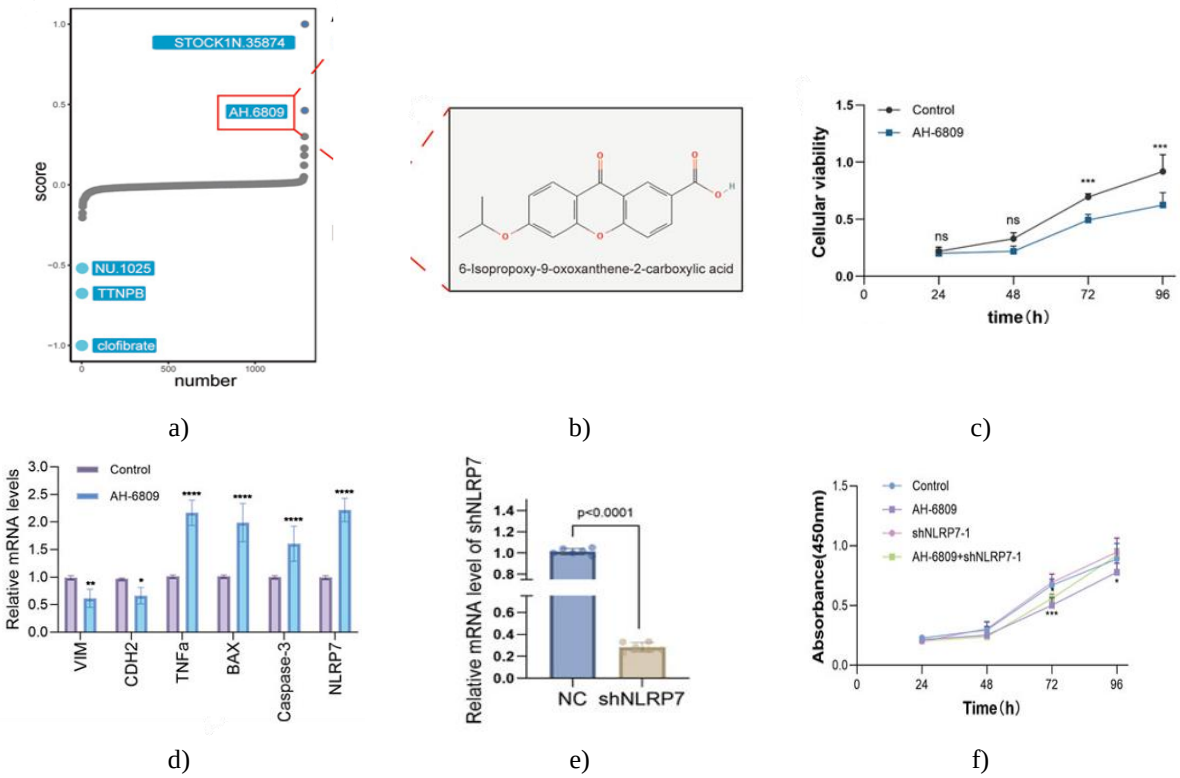

a) b) c)

d) e) f)

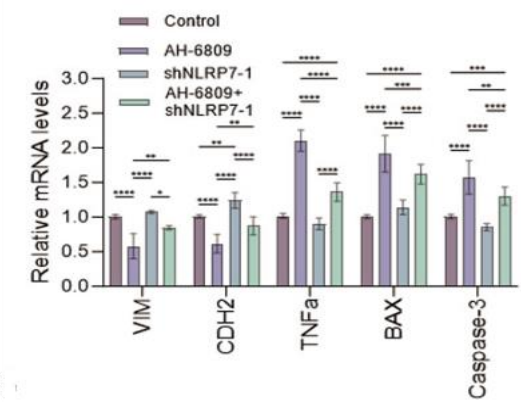

g)

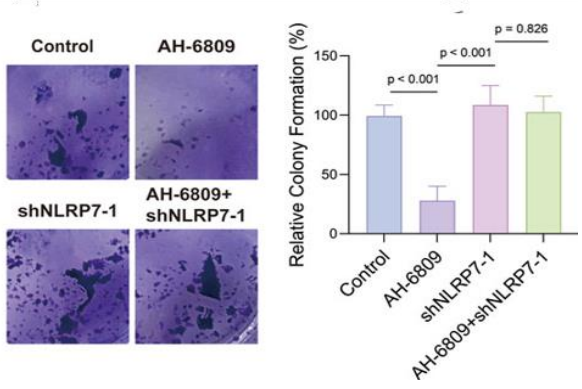

h)

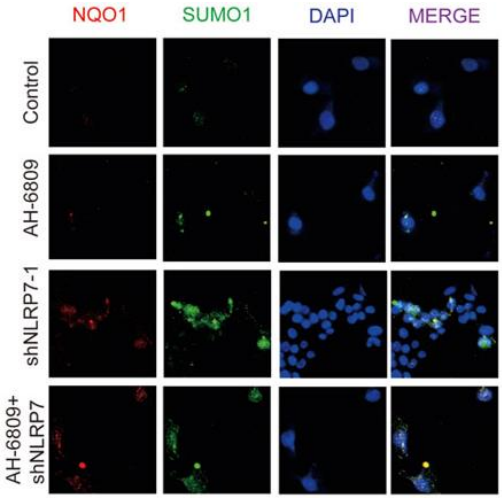

i)

Figure 6. AH-6809 modulates proliferation, apoptosis, and NLRP7-related pathways in LUAD cells. (a) High-throughput screening of a compound library identified AH-6809 as a candidate molecule affecting cell proliferation, apoptosis, and inflammatory signaling, leading to its selection for detailed investigation. (b) Chemical structure of AH-6809 (6-isopropoxy-8-oxosorban-2-carboxylic acid), illustrating the molecular configuration used in experimental assays. (c) CCK8 assay results showing the impact of AH-6809 on cell viability over 24, 48, 72, and 96 hours, revealing a significant time-dependent inhibition of proliferation (*$p < 0.05$, **$p < 0.01$, ***$p < 0.001$). (d) qRT-PCR analysis of key apoptotic (BAX, Caspase-3) and EMT/inflammatory markers (VIM, CDH2, TNFα) after AH-6809 treatment, demonstrating significant upregulation of pro-apoptotic and inflammatory genes and downregulation of EMT markers ($p < 0.001$). (e) Validation of shNLRP7 knockdown efficiency, with qRT-PCR showing marked reduction of NLRP7 mRNA compared to non-targeting control (NC) (**$p < 0.0001$). (f) CCK8 proliferation assay evaluating the combined effects of shNLRP7 knockdown and AH-6809 treatment over 96 hours, indicating reduced proliferation, which was further suppressed by AH-6809 (*$p < 0.001$). (g) qRT-PCR measurement of

apoptotic and EMT marker expression under four conditions: control, AH-6809 alone, shNLRP7 alone, and AH-6809 + shNLRP7, showing amplified pro-apoptotic gene expression and pronounced EMT inhibition in the combined treatment group ($p < 0.01$, ***$p < 0.001$). (h) Colony formation assay displaying the inhibitory effects of AH-6809 and shNLRP7 on long-term cell proliferation, with the combination treatment markedly reducing colony numbers. (i) Immunofluorescence analysis of inflammatory (NQO1) and anti-apoptotic (SUMO1) markers, with DAPI nuclear staining, highlighting enhanced apoptosis and inflammatory signaling in cells exposed to AH-6809, shNLRP7, or their combination.

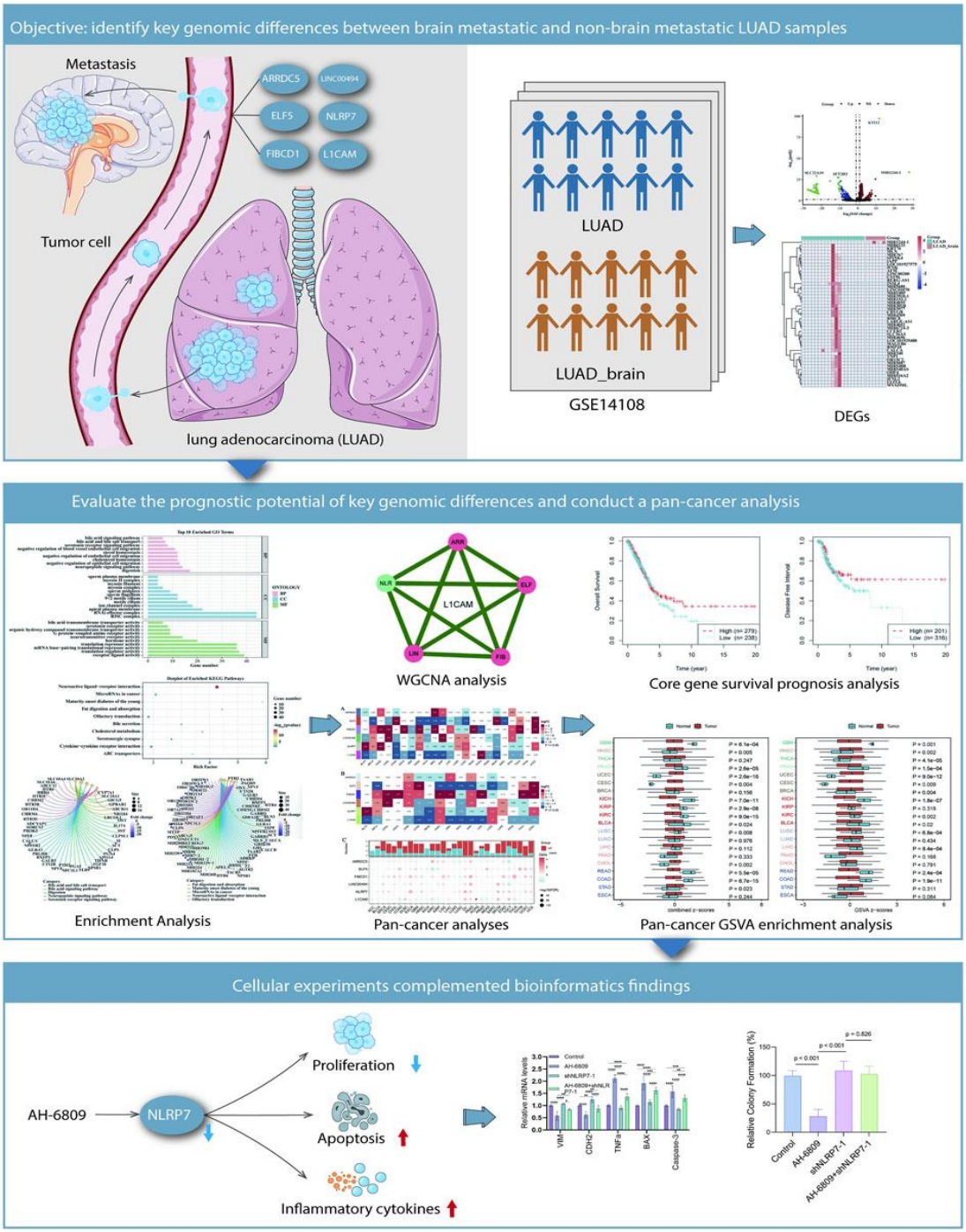

Figure 7. Overview of genomic alterations, cellular behaviors, and therapeutic effects in LUAD metastasis. The figure summarizes key findings on the interplay between genetic differences and cellular phenotypes in LUAD, highlighting the potential impact of AH-6809 and NLRP7. Analysis of LUAD datasets (GSE14108) revealed distinct gene expression patterns between brain-metastatic and non-brain-metastatic tumors, identifying genes such as FIBCD1, ELF5, and NLRP7 as significantly dysregulated. Heatmaps and bar charts

depict these differentially expressed genes (DEGs). Functional experiments supported these bioinformatics observations, showing that AH-6809 treatment partially counteracted molecular changes induced by NLRP7 knockdown, suggesting that the compound enhances NLRP7-mediated tumor-suppressive effects. The schematic illustrates the modulatory effects of AH-6809 and NLRP7 on cellular processes, including proliferation, apoptosis, reactive oxygen species (ROS) production, and expression of inflammatory cytokines.

This study explored the complex gene network underlying LUAD metastasis, identifying six key regulators: ARRDC5, ELF5, FIBCD1, LINC00494, NLRP7, and L1CAM, all of which influence tumor cell migration [17, 41]. A pan-cancer analysis further examined the expression patterns of these genes across multiple tumor types [18, 42], highlighting their potential utility as prognostic markers.

In LUAD, the expression levels of these genes correlated significantly with metastatic propensity. Elevated ARRDC5, FIBCD1, or ELF5 expression was predictive of higher metastatic risk in both non-IMI and IMI cohorts, consistent with results from our prognostic model. Pan-cancer evaluation also suggested that the downstream functions of genes like CCDC6 and PTK2 influence cellular behavior broadly across cancers, supporting prior evidence of their role in tumor progression. ARRDC5 and ELF5 were consistently associated with poor prognosis across diverse cancer types, suggesting their potential as universal prognostic biomarkers [42, 43].

Interestingly, L1CAM displayed an inverse correlation in metastatic LUAD compared to other cancers, where it is typically linked to invasion and migration [21, 44], underscoring context-dependent roles of this gene.

Although several of these genes—including ARRDC5, ELF5, FIBCD1, LINC00494, NLRP7, and L1CAM—have been implicated in cancer progression and metastasis [45-47], their specific contributions to LUAD brain metastasis remain incompletely understood. Our findings highlight the central role of NLRP7 in regulating inflammation and tumor immunity [24] and clarify that the involvement of L1CAM in LUAD invasiveness is more nuanced and context-dependent [48].

NLRP7 displays multifaceted functions in cancer, particularly in the context of LUAD brain metastasis [10, 49]. Our experiments revealed that LUAD patients with brain metastases exhibited markedly lower NLRP7 expression than those without, implying an inverse relationship between NLRP7 levels and the ability of lung cancer cells to cross the blood-brain barrier. Gene silencing experiments further showed that AH-6809 significantly suppressed cell proliferation and triggered apoptosis; however, this effect was reversed in NLRP7-deficient cells, highlighting NLRP7 as a critical regulator of tumor cell growth and programmed cell death. These findings suggest that NLRP7 may inhibit brain metastasis by modulating cell cycle progression and apoptotic pathways [50], and that AH-6809 could exert anti-metastatic effects by activating NLRP7. Collectively, NLRP7 represents a central modulator of LUAD cell survival and migration, making it a promising therapeutic target for preventing brain metastases.

As a member of the NOD-like receptor family, NLRP7 exerts diverse effects across multiple tumor types [10], regulating inflammatory responses, tumor growth, apoptosis, and the immune microenvironment. In ovarian cancer, NLRP7 influences cell survival through apoptosis and autophagy regulation, with low expression associated with increased tumor aggressiveness [51]. It also appears to mediate stress responses and chemoresistance in ovarian cancer cells [51]. In gastric cancer, diminished NLRP7 expression correlates with poor prognosis and higher tumor grade [52], while in breast cancer, NLRP7 affects tumor progression and metastasis by modulating immune cell infiltration and inflammation [53, 54]. In pancreatic cancer, low NLRP7 levels enhance anti-apoptotic capacity, further supporting its potential as a therapeutic target.

In parallel, SUMO1—a key factor in post-translational modification through SUMOylation—plays a pivotal role in regulating protein stability, localization, and function [55]. SUMOylation critically governs cell proliferation and apoptosis in tumors [56]. Our data indicate that AH-6809 treatment elevates SUMO1 expression in LUAD cells, suggesting that the compound may inhibit tumor growth by modulating apoptosis via SUMOylation pathways [57]. This may involve sustained activation of nuclear signaling cascades such as NF-κB and STAT3, which orchestrate cell survival and apoptotic processes [58]. Furthermore, AH-6809 enhances antioxidant defense by upregulating NQO1, supporting cellular homeostasis under stress. Together, these mechanisms point to AH-6809 as a promising therapeutic strategy in LUAD, warranting further preclinical and clinical investigation.

The emergence of targeted therapies in recent years has opened avenues for improving treatment efficacy while minimizing toxicity, driving advances in precision medicine [59]. Systematic reviews and meta-analyses have become invaluable tools for integrating data across drug development, bioinformatics, and translational research [60]. Concurrently, computer-aided drug design has accelerated novel compound discovery and highlighted new

therapeutic targets [60]. Research into cell death and metabolic regulation has similarly identified actionable targets for cancer therapy [61], enabling the development of highly specific interventions targeting proteins or genetic pathways [62]. For example, natural compounds like kiwi root extract suppress gastric cancer progression via the Wnt/β-catenin pathway [63], and combining modern technologies with traditional Chinese medicine provides additional opportunities for drug discovery [64].

Advances in materials science, photothermal therapy, and nanoparticle-based drug delivery have enhanced treatment efficacy, microenvironment modulation, and inflammation control [65-67]. "Off-the-shelf" gene therapy nanoparticles have expanded applications in regenerative medicine, including orthopedic and soft tissue repair [68]. Improved drug delivery and nanotechnology approaches have increased therapeutic specificity and efficacy [69], demonstrating the value of interdisciplinary approaches in disease management. Integrated data analysis and multidimensional evaluation are increasingly essential in modern medicine [70, 71]. Additionally, social support plays a crucial role in cancer patient mental health, particularly in Chinese populations [72, 73].

Identifying genes that are critically involved in LUAD metastasis and exhibit prognostic value across various cancer types will facilitate the development of precision oncology [4, 74]. Molecular classification of metastatic potential and patient prognosis through gene expression profiling is essential for tailoring individualized treatment approaches [75, 76]. Our results offer novel mechanistic insights into how these genes influence tumor progression, particularly by modulating the tumor microenvironment and host immune responses, thereby opening new avenues for therapeutic investigation [66, 77].

Given that the present study is retrospective and relies on a relatively modest sample size, certain biases may be present in our conclusions [78, 79], Furthermore, although the use of publicly available datasets provides broad and valuable information, it may limit the granularity of the analysis [80, 81]. Potential confounding factors include heterogeneity in data acquisition protocols, differences in patient demographics, and variable data quality control. Consequently, additional experimental validation is required to definitively elucidate the functional contributions of these genes to LUAD metastasis [27, 82]. Larger, more diverse patient cohorts in future studies will be instrumental in confirming our observations and translating these genes into clinically actionable biomarkers or therapeutic targets [16 , 17].

Prospective research should therefore incorporate diverse populations, integrate independent datasets, and apply consistent analytical pipelines across cohorts to assess the robustness of our findings. Moreover, detailed in vitro functional assays and in vivo animal models represent critical next steps.

In summary, our work illuminates complex gene regulatory networks underlying LUAD metastasis and extends these insights to a pan-cancer context. By integrating genomic, epigenomic, and transcriptomic data, we identified ARRDC5, ELF5, FIBCD1, LINC00494, NLRP7, and L1CAM as candidate prognostic markers applicable to multiple malignancies [83, 84]. These findings substantially enhance our understanding of cancer biology [85, 86]. Despite the inherent limitations of our study, it lays a strong groundwork for subsequent investigations and holds promise for informing clinical decision-making, ultimately contributing to better patient outcomes [87, 88]. Further validation studies are essential to corroborate these results and explore their translational and therapeutic implications, paving the way toward more precise and effective cancer therapies [89, 90].

Conclusion

In this research, NLRP7, ELF5, FIBCD1, ARRDC5, LINC00494, and L1CAM were recognized as pivotal prognostic biomarkers for LUAD metastasis, with a particular emphasis on brain dissemination, and NLRP7 was identified as a major driver of metastatic progression. AH-6809 demonstrated therapeutic promise by reducing LUAD cell growth, promoting apoptosis, and regulating critical pathways, including SUMO1-dependent post-translational modifications and NQO1 activity. These observations suggest that interventions targeting NLRP7 and its downstream mechanisms could represent novel strategies to curb LUAD metastasis, warranting further experimental validation and clinical exploration to substantiate their potential applications.

Acknowledgments: We used ChatGPT-4.0 for language editing to improve the accuracy and fluency of the manuscript. The tool was employed solely for grammatical correction and language optimization, and it did not contribute to the design of the study, data analysis, or interpretation of the results. Therefore, the use of this tool complies with academic ethical standards and does not compromise the independence or validity of the research.

Conflict of Interest: None

Financial Support: The author(s) declare that financial support was received for the research, authorship, and/or publication of this article. This study was supported by the project “Clinical Research on the Impact of ALK Inhibitors on Brain Metastasis in Non-Small Cell Lung Cancer” (JZ 2023B036).

Ethics Statement: None

References

1. Sainz De Aja J, Dost AFM, Kim CF. Alveolar progenitor cells and the origin of lung cancer. J Intern Med. 2021;289(5):629-35.
2. Ye J, Liu H, Xu Z, Zheng L, Liu R. Identification of a multidimensional transcriptome prognostic signature for lung adenocarcinoma. J Clin Lab Anal. 2019;33(9):e22990.
3. Webb JD, Simon MC. Novel insights into the molecular origins and treatment of lung cancer. Cell Cycle. 2010;9(20):4098-105.
4. Li L, Peng M, Xue W, Fan Z, Wang T, Lian J, et al. Integrated analysis of dysregulated long non-coding RNAs/microRNAs/mRNAs in metastasis of lung adenocarcinoma. J Transl Med. 2018;16(1):372.
5. Yang J, Mani SA, Donaher JL, Ramaswamy S, Itzykson RA, Come C, et al. Twist, a master regulator of morphogenesis, plays an essential role in tumor metastasis. Cell. 2004;117(7):927-39.
6. Valastyan S, Weinberg RA. Tumor metastasis: molecular insights and evolving paradigms. Cell. 2011;147(2):275-92.
7. Shi J, Hua X, Zhu B, Ravichandran S, Wang M, Nguyen C, et al. Somatic genomics and clinical features of lung adenocarcinoma: a retrospective study. PLoS Med. 2016;13(12):e1002162.
8. Kleczko EK, Kwak JW, Schenk EL, Nemenoff RA. Targeting the complement pathway as a therapeutic strategy in lung cancer. Front Immunol. 2019;10:954.
9. Chen X, Bu Q, Yan X, Li Y, Yu Q, Zheng H, et al. Genomic mutations of primary and metastatic lung adenocarcinoma in Chinese patients. J Oncol. 2020;2020:6615575.
10. Li D, Huang Y, Cai L, Wu M, Bao H, Xu Y, et al. Genomic landscape of metastatic lung adenocarcinomas from large-scale clinical sequencing. Neoplasia. 2021;23(12):1204-12.
11. Xie S, Wu Z, Qi Y, Wu B, Zhu X. The metastasizing mechanisms of lung cancer: recent advances and therapeutic challenges. Biomed Pharmacother. 2021;138:111450.
12. Liu Z, Zhang S. Toward a systematic understanding of cancers: a survey of the pan-cancer study. Front Genet. 2014;5:194.
13. Mastrogiacomo B, Dunne EG, Fick CN, Nguyen J, Hathwar J, Lankadasari M, et al. Abstract 2556: longitudinal analyses of clinical sequencing data provide novel insights into the evolutionary dynamics of lung adenocarcinoma. Cancer Res. 2024;84(6_Supplement):2556.
14. Testa U, Pelosi E, Castelli G. Molecular charcterization of lung adenocarcinoma combining whole exome sequencing, copy number analysis and gene expression profiling. Expert Rev Mol Diagn. 2022;22(1):77-100.
15. Mardis ER. Clinical and genomic insights from metastatic cancers. Clin Chem. 2018;64(5):766-8.
16. Minn AJ, Gupta GP, Siegel PM, Bos PD, Shu W, Giri DD, et al. Genes that mediate breast cancer metastasis to lung. Nature. 2005;436(7050):518-24.
17. Yao X, Zhang H, Tang S, Zheng X, Jiang L. Bioinformatics analysis to reveal potential differentially expressed long non-coding RNAs and genes associated with tumour metastasis in lung adenocarcinoma. Onco Targets Ther. 2020;13:3197-207.
18. Mishra S, Kaddi CD, Wang MD. Pan-cancer analysis for studying cancer stage using protein and gene expression data. In: 2016 38th Annual International Conference of the IEEE Engineering in Medicine and Biology Society (EMBC). Orlando, FL, USA: IEEE; 2016. p. 2440-3.
19. Piggin CL, Roden DL, Gallego-Ortega D, Lee HJ, Oakes SR, Ormandy CJ. ELF5 isoform expression is tissue-specific and significantly altered in cancer. Breast Cancer Res. 2016;18(1):4.
20. Wu S-G, Chang T-H, Liu Y-N, Shih J-Y. MicroRNA in lung cancer metastasis. Cancers (Basel). 2019;11(2):265.

21. Hai J, Zhu C-Q, Bandarchi B, Wang Y-H, Navab R, Shepherd FA, et al. L1 cell adhesion molecule promotes tumorigenicity and metastatic potential in non–small cell lung cancer. Clin Cancer Res. 2012;18(7):1914-24.
22. Guo H, Zhang J, Qin C, Yan H, Liu T, Hu H, et al. Biomarker-targeted therapies in non–small cell lung cancer: current status and perspectives. Cells. 2022;11(20):3200.
23. Yamaguchi M, Hirai S, Idogawa M, Sumi T, Uchida H, Sakuma Y. A newly developed anti-L1CAM monoclonal antibody targets small cell lung carcinoma cells. Int J Mol Sci. 2024;25(16):8748.
24. Feng A, Li Y, Li G, Wang Y, Wen Q, Yang Z, et al. Genomic features of organ-specific metastases in lung adenocarcinoma. Front Oncol. 2022;12:908759.
25. Näpflin K, O'Connor EA, Becks L, Bensch S, Ellis VA, Hafer-Hahmann N, et al. Genomics of host-pathogen interactions: challenges and opportunities across ecological and spatiotemporal scales. PeerJ. 2019;7:e8013.
26. Liang SG, Greenwood TA. The impact of clinical heterogeneity in schizophrenia on genomic analyses. Schizophr Res. 2015;161(2-3):490-5.
27. Wang J, Chen T, Yu X, Ouyang N, Tan L, Jia B, et al. Identification and validation of smoking-related genes in lung adenocarcinoma using an in vitro carcinogenesis model and bioinformatics analysis. J Transl Med. 2020;18(1):313.
28. Zhang D, Jiang Q, Ge X, Shi Y, Ye T, Mi Y, et al. RHOV promotes lung adenocarcinoma cell growth and metastasis through JNK/c-Jun pathway. Int J Biol Sci. 2021;17(10):2622-32.
29. Takano T, Ito M. An extensive basal ganglia hemorrhage in a preexisting neonatal asphyxiated lesion after mRNA-based SARS-CoV-2 vaccination: a fatal adult case of cerebral palsy. Brain Hemorrhages. 2023;5:38-41.
30. Yuan J, Liao Y, Zhang T, Tang Y, Yu P, Liu Y, et al. Integrating bulk RNA and single-cell sequencing data unveils efferocytosis patterns and ceRNA network in ischemic stroke. Transl Stroke Res. 2024;16(3):733-46.
31. Wu H, Wang F, Yang L, Chen L, Tang J, Liu Y, et al. Carboxymethyl chitosan promotes biofilm-formation of Cryptococcus laurentii to improve biocontrol efficacy against Penicillium expansum in grapefruit. Adv Compos Hybrid Mater. 2024;7:23.
32. Tian Z, Liu J, Zeng M, Zeng Q. Tong jing Yi Hao formula alleviates ornidazole-induced oligoasthenospermia in rats by suppressing ROS/MAPK/HIF-1 pathway. Arch Esp Urol. 2023;76(8):596-604.
33. Cao Z, Pang Y, Pu J, Liu J. Bacteria-based drug delivery for treating non-oncological diseases. J Control Release. 2024;366:668-83.
34. Zhao L, Hu H, Zhang L, Liu Z, Huang Y, Liu Q, et al. Inflammation in diabetes complications: molecular mechanisms and therapeutic interventions. MedComm (2020). 2024;5(4):e516.
35. Thakur A, Banerjee R, Thakur S, Kumar G, Thakur SS. Role of macrophage polarization in cancer progression and their association with COVID-19 severity. Cancer Insight. 2023;2(1):68-79.
36. Wu X, Jing Z, Huang T, Jing Y. BOP1 promotes prostate cancer through the DUSP6/MAPK pathway. Arch Esp Urol. 2023;76(6):445-53.
37. Zhuo Z, Zhang D, Lu W, Wu X, Cui Y, Zhang W, et al. Reversal of tamoxifen resistance by artemisinin in ER+ breast cancer: bioinformatics analysis and experimental validation. Oncol Res. 2024;32(6):1093-107.
38. Aydoğdu YF, Gülçek E, Büyükkasap Ç, Bostancı H. Outcomes of thyroidectomy for secondary thyroid malignancies, a single center experience. Discov Onc. 2024;15:104.
39. Yang C, Zhang H, Chen M, Wang S, Qian R, Zhang L, et al. A survey of optimal strategy for signature-based drug repositioning and an application to liver cancer. eLife. 2022;11:e71880.
40. Malta TM, Sokolov A, Gentles AJ, Burzykowski T, Poisson L, Weinstein JN, et al. Machine learning identifies stemness features associated with oncogenic dedifferentiation. Cell. 2018;173(2):338-54.e15.
41. Zhang S, Lu Y, Liu Z, Li X, Wang Z, Cai Z. Identification six metabolic genes as potential biomarkers for lung adenocarcinoma. J Comput Biol. 2020;27(10):1532-43.
42. Anaya J, Reon B, Chen WM, Bekiranov S, Dutta A. A pan-cancer analysis of prognostic genes. PeerJ. 2016;3:e1499.
43. Nagy Á, Munkácsy G, Győrffy B. Pancancer survival analysis of cancer hallmark genes. Sci Rep. 2021;11(1):6047.

44. Tischler V, Pfeifer M, Hausladen S, Schirmer U, Bonde AK, Kristiansen G, et al. L1CAM protein expression is associated with poor prognosis in non-small cell lung cancer. Mol Cancer. 2011;10:127.
45. Altevogt P, Ben-Ze'ev A, Gavert N, Schumacher U, Schäfer H, Sebens S. Recent insights into the role of L1CAM in cancer initiation and progression. Int J Cancer. 2020;147(12):3292-6.
46. Graca FA, Rai M, Hunt LC, Stephan A, Wang YD, Gordon B, et al. The myokine Fibcd1 is an endogenous determinant of myofiber size and mitigates cancer-induced myofiber atrophy. Nat Commun. 2022;13(1):2370.
47. Luk IY, Reehorst CM, Mariadason JM. ELF3, ELF5, EHF and SPDEF transcription factors in tissue homeostasis and cancer. Molecules. 2018;23(9):2191.
48. Wang JW, Wang HL, Liu Q, Hu K, Yuan Q, Huang SK, et al. L1CAM expression in either metastatic brain lesion or peripheral blood is correlated with peripheral platelet count in patients with brain metastases from lung cancer. Front Oncol. 2022;12:990762.
49. Lin L, Chen Y, Wu B, Chen Y, Li Z. Identification of the pyroptosis-related prognostic gene signature and the associated regulation axis in lung adenocarcinoma. Cell Death Discov. 2021;7(1):161.
50. Reynaud D, Alfaidy N, Collet C, Lemaitre N, Sergent F, Miege C, et al. NLRP7 enhances choriocarcinoma cell survival and camouflage in an inflammasome independent pathway. Cells. 2023;12(6):857.
51. Mamoor S. Mamoor S. Expression of the interleukin-1 receptor antagonist associates with patient survival in high-grade serous ovarian cancer. 2020.
52. Jiang Z, Yu T, Fan Z, Yang H, Lin X. Krüppel-like factor 7 is a marker of aggressive gastric cancer and poor prognosis. Cell Physiol Biochem. 2017;43(3):1090-9.
53. Ershaid N, Sharon Y, Doron H, Raz Y, Shani O, Cohen N, et al. NLRP3 inflammasome in fibroblasts links tissue damage with inflammation in breast cancer progression and metastasis. Nat Commun. 2019;10(1):4375.
54. Lee JY, Lee HE, Yang G, Kang HC, Cho YY, Lee HS. NLRP3 inflammasome in immune cells regulates metastatic potential of cancer. J Immunol. 2020;204(1 Supplement):68.27.
55. Barry J, Lock RB. Small ubiquitin-related modifier-1: wrestling with protein regulation. Int J Biochem Cell Biol. 2011;43(1):37-40.
56. Gong L, Qi R, Li D. Sumoylation pathway as potential therapeutic targets in cancer. Curr Mol Med. 2017;16(9):900-5.
57. Ke C, Zhu K, Sun Y, Ni Y, Zhang Z, Li X. SUMO1 promotes the proliferation and invasion of non-small cell lung cancer cells by regulating NF-κB. Thorac Cancer. 2019;10(1):33-40.
58. Fan Y, Mao R, Yang J. NF-κB and STAT3 signaling pathways collaboratively link inflammation to cancer. Protein Cell. 2013;4(3):176-85.
59. Vargas-Sierra O, Hernández-Juárez J, Uc-Uc PY, Herrera LA, Domínguez-Gómez G, Gariglio P, et al. Role of SLC5A8 as a tumor suppressor in cervical cancer. Front Biosci (Landmark Ed). 2024;29(1):16.
60. Wu Z, Chen S, Wang Y, Li F, Xu H, Li M, et al. Current perspectives and trend of computer-aided drug design: a review and bibliometric analysis. Int J Surg. 2024;110(6):3848-78.
61. Lin WJ, Shi WP, Ge WY, Chen LL, Guo WH, Shang P, et al. Magnetic fields reduce apoptosis by suppressing phase separation of Tau-441. Research (Wash D C). 2023;6:0146.
62. Hong W, Lei H, Peng D, Huang Y, He C, Yang J, et al. A chimeric adenovirus-vectored vaccine based on Beta spike and Delta RBD confers a broad-spectrum neutralization against Omicron-included SARS-CoV-2 variants. MedComm (2020). 2024;5(4):e539.
63. Chu YM, Huang QY, Wang TX, Yang N, Jia XF, Shi ZM, et al. Actinidia chinensis Planch. root extract downregulates the Wnt/β-catenin pathway to treat gastric cancer: a mechanism study based on network pharmacology. Tradit Med Res. 2023;8:40.
64. Wang FC, Han P, Li H, Ye HY, Zhou PX, Tian W, et al. Advantages and prospects of traditional Chinese medicine in treating COVID-19. Tradit Med Res. 2023;8:22.
65. Shi Z, Bai H, Wu J, Miao X, Gao J, Xu X, et al. Acceptor engineering produces ultrafast nonradiative decay in NIR-II aza-BODIPY nanoparticles for efficient osteosarcoma photothermal therapy via concurrent apoptosis and pyroptosis. Research (Wash D C). 2023;6:0169.
66. Yang J, Xu J, Wang W, Zhang B, Yu X, Shi S. Epigenetic regulation in the tumor microenvironment: molecular mechanisms and therapeutic targets. Signal Transduct Target Ther. 2023;8(1):210.

67. Wu H, Wang F, Yang L, Chen L, Tang J, Liu Y, et al. Carboxymethyl chitosan promotes biofilm-formation of Cryptococcus laurentii to improve biocontrol efficacy against Penicillium expansum in grapefruit. Adv Compos Hybrid Mater. 2024;7:23.
68. O'Shea D, Hodgkinson T, Dixon J, Curtin C, O'Brien F. Development of an "off-the-shelf" gene therapeutic nanoparticle formulation for incorporation into biomaterials for regenerative medicine applications. Eur Cell Mater. 2024;47:152-69.
69. Romanovska A, Schmidt M, Brandt V, Tophoven J, Tiller JC. Controlling the function of bioactive worm micelles by enzyme-cleavable non-covalent inter-assembly cross-linking. J Control Release. 2024;368:15-23.
70. Oinaka H, Kawakita F, Nakajima H, Suzuki Y, Nampei M, Okada T, et al. Increased plasma periostin concentration predicts angiographic vasospasm development in non-severe aneurysmal subarachnoid hemorrhage. Brain Hemorrhages. 2024;5:1-7.
71. Latini E, Nusca S, Curci E, Boaretto D, Santoboni F, Trischitta D, et al. Intramuscular paravertebral oxygen-ozone therapy for chronic neck pain and low back pain: evaluation of 6-month clinical outcomes. Med Gas Res. 2024;14(1):6-11.
72. Zhu W. The impact of social support on the mental health of cancer patients: evidence from China. PO. 2024;18:69-77.
73. Paillard-Brunet G, Couillet A. Peer-Support in Oncology: A Qualitative Study of Caregivers Perception in a Cancer Center. PO. 2024;18:23-31.
74. Liu D, Yao L, Ding X, Zhou H. Multi-omics immune regulatory mechanisms in lung adenocarcinoma metastasis and survival time. Comput Biol Med. 2023;164:107333.
75. Bustin SA, Dorudi S. Gene expression profiling for molecular staging and prognosis prediction in colorectal cancer. Expert Rev Mol Diagn. 2004;4(5):599-607.
76. Van'T Veer LJ, Dai H, Van De Vijver MJ, He YD, Hart AAM, Mao M, et al. Gene expression profiling predicts clinical outcome of breast cancer. Nature. 2002;415(6871):530-6.
77. Andrews MC, Reuben A, Gopalakrishnan V, Wargo JA. Concepts collide: genomic, immune, and microbial influences on the tumor microenvironment and response to cancer therapy. Front Immunol. 2018;9:946.
78. Lin L. Bias caused by sampling error in meta-analysis with small sample sizes. PLoS One. 2018;13(9):e0204056.
79. Zhou JY. Bias in the proportionate mortality ratio analysis of small study populations: a case on analyses of radiation and mesothelioma. Int J Radiat Biol. 2014;90(12):1075-9.
80. Altamimi E, Al-Ali A, Malluhi QM, Al-Ali AK. Smart grid public datasets: characteristics and associated applications. IET Smart Grid. 2024;7(5):503-30.
81. Phillippi JC, Neal JL, Carlson NS, Biel FM, Snowden JM, Tilden EL. Utilizing datasets to advance perinatal research. J Midwifery Womens Health. 2017;62(5):545-61.
82. Cheng WC, Chang CY, Lo CC, Hsieh CY, Kuo TT, Tseng GC, et al. Identification of theranostic factors for patients developing metastasis after surgery for early-stage lung adenocarcinoma. Theranostics. 2021;11(8):3661-75.
83. Zhao Q, Shi X, Xie Y, Huang J, Shia B, Ma S. Combining multidimensional genomic measurements for predicting cancer prognosis: observations from TCGA. Brief Bioinform. 2015;16(2):291-303.
84. Zhu B, Song N, Shen R, Arora A, Machiela MJ, Song L, et al. Integrating clinical and multiple omics data for prognostic assessment across human cancers. Sci Rep. 2017;7(1):16954.
85. Paltridge JL, Belle L, Khew-Goodall Y. The secretome in cancer progression. Biochim Biophys Acta. 2013;1834(11):2233-41.
86. Nicolini A. Experimental and clinical advances in counteracting progression of solid cancers. Cancers (Basel). 2023;15(7):1956.
87. Jeffs L, Muntlin Athlin A, Needleman J, Jackson D, Kitson A. Building the foundation to generate a fundamental care standardised data set. J Clin Nurs. 2018;27(13-14):2481-8.
88. Ferrill MJ, FakhriRavari A, Hong L, Wedret JJ. A focus on evaluating major study limitations in order to apply clinical trials to patient care: implications for the healthcare team. Hosp Pharm. 2021;56(6):597-603.
89. Ledermann JA, Canevari S, Thigpen T. Targeting the folate receptor: diagnostic and therapeutic approaches to personalize cancer treatments. Ann Oncol. 2015;26(10):2034-43.

90. Kamel HFM, Al-Amodi HSAB. Exploitation of gene expression and cancer biomarkers in paving the path to era of personalized medicine. Genom Proteom Bioinform. 2017;15(4):220-35.